Journal of Catalysis 279 (2011) 27–35

Contents lists available at ScienceDirect

Journal of Catalysis

journal homepage: www.elsevier.com/locate/jcat

Citric acid-assisted hydrothermal method for preparing NiW/USY–Al_2O_3ultradeep hydrodesulfurization catalysts

Yu Fan [a,b], Han Xiao [b], Gang Shi [b], Haiyan Liu [b], Ying Qian [c], Tinghai Wang [c], Guangbi Gong [c], Xiaojun Bao [a,b,*]

[a] State Key Laboratory of Heavy Oil Processing, China University of Petroleum, No. 18 Fuxue Rd., Beijing 102249, People's Republic of China
[b] The Key Laboratory of Catalysis, China National Petroleum Corporation, China University of Petroleum, No. 18 Fuxue Rd., Beijing 102249, People's Republic of China
[c] Lanzhou Research Center, Petrochemical Research Institute, PetroChina Company Ltd., No. 1 Heshuibeilu, Xigu District, Lanzhou 730060, People's Republic of China

ARTICLE INFO

Article history:
Received 26 August 2010
Revised 21 December 2010
Accepted 23 December 2010
Available online 12 February 2011

Keywords:
Citric acid
Hydrothermal dispersion
Hydrothermal modification
NiW/USY–Al_2O_3
Hydrodesulfurization catalysts

ABSTRACT

This article presents a novel method for preparing NiW/USY–Al_2O_3 ultradeep hydrodesulfurization (HDS) catalysts via combined citric acid-assisted hydrothermal dispersion of active metals and hydrothermal modification of HY zeolite. The results showed that the citric acid-assisted hydrothermal method yielded monomeric W species as W precursors that were well dispersed by the interaction between citric acid and WO_3 particles and were suitably stacked by the preferential interaction between citric acid and the support, guaranteeing a compromised dispersion and stacking of the supported Ni–W–S phases. The citric acid-assisted hydrothermal modification combined the framework dealumination of the HY zeolite and the removal of nonframework Al species, exposing more Brønsted acid sites on the catalyst. The finely tuned morphology of the Ni–W–S phases and the suitably adjusted Brønsted acidity of the zeolite endowed the resulting NiW/USY–Al_2O_3 catalyst with outstanding hydrogenation and hydrogenolysis activities for 4,6-dimethyldibenzothiophene and coking diesel HDS.

1. Introduction

Sulfur-containing compounds in transportation fuels such as gasoline and diesel are closely related to SO_x and particle emissions from internal combustion engines that result in air pollution and acid rain, so both developed and developing countries have strictly restricted sulfur content in their environmental regulations. Hydrodesulfurization (HDS) is the most widely used technique for removing sulfur-containing compounds from petroleum and petroleum processing products in the refining industry [1]. In various HDS processes, HDS catalysts play a pivotal role in determining the processes' features and efficiency. As the most important type of HDS catalysts, alumina-supported Mo and W catalysts with Co or/and Ni as promoting elements have been used in the refining industry for more than half a century, but they show poor ability to remove 4,6-dimethyldibenzothiophene (4,6-DMDBT), which is the most refractory sulfur-containing compound in transportation fuels, because of its steric hindrance for direct HDS [2]. Therefore, extensive efforts have been made to develop HDS catalysts with improved activity for the conversion of 4,6-DMDBT. Two principal pathways are explored to overcome the steric hindrance of the methyl groups at the 4 and 6 positions in 4,6-DMDBT.

The first pathway is based on the well-documented fact that HDS of 4,6-DMDBT occurs preferentially via the hydrogenation route involving the chemisorption of 4,6-DMDBT through the π electrons of the aromatic rings in a flat mode parallel to the catalyst surface, the hydrogenation of one benzenic ring in 4,6-DMDBT, and the subsequent desulfurization of this prehydrogenated intermediate [3]. To improve the hydrogenation function of conventional supported Mo or W HDS catalysts, several methods have been proposed, with some of them having been employed in industrial practice. Using alternative unitary supports such as carbon [4], titania [5], zirconia [6], and silica [7] and binary supports such as TiO_2–Al_2O_3 [8], SiO_2–Al_2O_3 [9], and ZrO_2–Al_2O_3 [10] is such a method. Compared to Al_2O_3-supported HDS catalysts, the catalysts based on these unitary and binary supports show enhanced HDS activity, but suffer from the problem of inferior mechanical strength or undesirable agglomeration of supported active metals [11]. Modification of Al_2O_3 by incorporating phosphorus [12], fluorine [13], and chelating agents such as ethylenediaminetetraacetic acid (EDTA), nitrilotriacetic acid (NTA), and 1,2-cyclohexanediamine-*N,N,N,N*-tetraacetic acid (CyNTA) [14,15], has been also attempted, but this leads to the formation of larger active metal particles with lower dispersion, decreasing the number of active sites and giving unsatisfactory HDS performance [16]. In addition, it has been recognized that the electronic properties of active sulfide phases in the vicinity of acidic sites of β and Y zeolites might be modified, and the modification can increase the catalyst's activity for hydrogenating the benzenic rings in sulfur-containing compounds [17,18].

* Corresponding author at: State Key Laboratory of Heavy Oil Processing, China University of Petroleum, No. 18 Fuxue Rd., Beijing 102249, People's Republic of China. Fax: +86(0) 10 89734979.
E-mail address: baoxj@cup.edu.cn (X. Bao).

0021-9517/$ - see front matter © 2010 Elsevier Inc. All rights reserved.
doi:10.1016/j.jcat.2010.12.014

The second pathway to improving the elimination of sulfur from 4,6-DMDBT is the structural modification of 4,6-DMDBT through isomerization or cracking of methyl groups from positions 4 and 6. By shifting one of the two substituent methyl groups from the 4 or 6 position to the 3 or 7 position through hydroisomerization [19], or by the removal of one or both methyl groups through dealkylation [20], the steric hindrance existing in 4,6-DMDBT can be relieved, promoting the occurrence of HDS reactions of 4,6-DMDBT. To fulfill this task, acidic zeolites that have excellent isomerization and dealkylation performance have been incorporated into conventional alumina supports [21]. Compared to microporous zeolites such as HY and Hβ, which usually have stronger acidity and thus show excessive cracking and rapid deactivation [22], ultrastable zeolite Y (USY) obtained by hydrothermally treating HY zeolite presents decreased acid strength [23] and well-developed secondary mesopores [24] and thus is more attractive for the HDS of 4,6-DMDBT because of its stable HDS activity and appropriate pore channels for the diffusion and reaction of large sulfur-containing compounds [25]. Unfortunately, when conventional impregnation is adopted for loading molybdenum or tungsten onto zeolite-containing supports, poor dispersion of the deposited phase is encountered [26,27].

The above discussions clearly suggest that an effective route to design and fabrication of highly efficient HDS catalysts is incorporation of USY into conventional γ-Al_2O_3 and improvement of the dispersion of active metals on the resulting composite support. For this purpose, we present a novel method for preparing NiW/USY–Al_2O_3 ultradeep HDS catalysts. The method was achieved by coupling the citric acid-assisted hydrothermal dispersion of supported active metals and the hydrothermal modification of HY zeolite (CHD-HMY). It was shown that (1) by using citric acid as a dispersant in aqueous solutions under hydrothermal conditions to control the size of W precursors and weaken the metal–support interaction, a compromise between the dispersion and stacking of supported W species was fulfilled; (2) the pore structure and acidity of incorporated USY zeolite were simultaneously modified during the hydrothermal process, avoiding the complex post-treatments encountered in conventional modifications.

2. Experimental

2.1. Catalyst preparation

Two NiW/USY–Al_2O_3 catalysts, designated as CHD-HMY and IWI, were prepared by the CHD-HMY method proposed in this investigation and the incipient wetness impregnation method (IWI), respectively.

2.1.1. Preparation of catalyst CHD-HMY

The preparation of the oxidic catalyst CHD-HMY involves the following steps. First, the calcined HY zeolite (molar Si/Al ratio 2.6, unit cell parameter 24.68 Å, surface area 710 m^2/g, pore volume 0.34 mL/g, Qilu Catalyst Factory, People's Republic of China) was fully blended with pseudo-boehmite (surface area 250 m^2/g, pore volume 0.60 ml/g, Shandong Aluminum Plant, People's Republic of China) in a dry mass ratio of 21:79 by grinding and shaped by extrusion. After they were dried at 120 °C for 4 h and calcined at 450 °C for 4 h, the extrudates were crushed and screened to obtain 20–40 mesh particles. Second, 6.0 g of the HY–Al_2O_3 particles was added into 37.9 ml of a 0.50 M citric acid solution and then 61.8 ml of a 0.15 M sodium tungstate solution was added under stirring. Third, 27.1 ml of a 0.70 M HCl solution was added dropwise into the above solution under stirring and the resulting suspension was transferred to a rotary Teflon-lined stainless steel autoclave and heated at 140 °C for 15 h. Fourth, the as-prepared product was filtered, washed with deionized water, dried at 120 °C for 2 h, and calcined at 450 °C for 4 h under N_2. Finally, the obtained W/USY–Al_2O_3 product was impregnated with a suitable amount of nickel nitrate solution and dried and calcined as mentioned above.

2.1.2. Preparation of catalyst IWI

The oxidic catalyst IWI was prepared as follows. First, the calcined HY zeolite was hydrothermally treated in a rotary Teflon-lined stainless steel autoclave at 140 °C for 15 h. Second, the treated HY zeolite (USY) was fully blended with pseudo-boehmite at a dry mass ratio of 21:79 by grinding and shaped by extrusion. Finally, the dried and calcined 20–40 mesh extrudates were impregnated successively with the aqueous solutions of ammonium metatungstate and nickel nitrate according to the required loadings; after each impregnation step, the solids were dried and calcined as mentioned above.

To clarify the effect of citric acid on supported active metals in IWI, one catalyst, denoted as IWI-IC, was prepared by adding the same amount of citric acid as used for preparing catalyst CHD-HMY into the impregnation solution for preparing catalyst IWI.

To elucidate the benefit of the CHD-HMY method, one more catalyst, denoted as IWI-HC, was prepared by adding the same amount of citric acid as used for preparing catalyst CHD-HMY into the hydrothermal solution for producing the USY zeolite used in catalyst IWI.

To understand the important role of citric acid in the CHD-HMY method, a reference catalyst denoted as HD-HMY was prepared according to the same procedure as that for preparing catalyst CHD-HMY except for the absence of citric acid.

The NiO and WO_3 contents in all of the NiW/USY–Al_2O_3 catalysts determined by X-ray fluorescence spectroscopy (XRF, Rigaku ZSX-100e) were 3.0 and 26.0 wt.%, respectively. All of the USY–Al_2O_3 supports consist of 21 wt.% USY and 79 wt.% Al_2O_3. In the present investigation, W and Ni were selected as the supported active metals because the Ni–W system has the highest hydrogenation activity among the four possible metal combinations of Mo or W with Co or Ni [28].

2.2. Catalyst characterization

Temperature-programmed reduction (TPR) analyses of the oxidic catalysts were performed on a homemade apparatus. First, the catalyst samples (each 100 mg) to be tested were pretreated in an Ar stream at 450 °C for 2 h and then cooled to room temperature. Then, the Ar flow was switched to a 10% H_2/Ar flow, and the catalyst sample was heated to 1050 °C at a rate of 10 °C/min and kept at this temperature for 0.5 h. The H_2 consumption for reducing the corresponding metal oxides in the catalyst was detected by a thermal conductivity detector (TCD).

The types of acid sites were determined by pyridine-adsorbed Fourier transformed infrared (Py-FTIR) experiments conducted on a Magna 560 FT-IR instrument. A wafer of an oxidic catalyst was introduced into the FT-IR cell and sulfided in situ in a 15% H_2S/H_2 stream at 360 °C for 2 h. After sulfidation, the H_2S-containing gas mixture and chemisorbed H_2S were removed by flushing the cell with purified He at 360 °C for 2 h. Then the sample was slowly cooled to ambient temperature in a purified He flow and evacuated to 1.33×10^{-3} Pa, followed by the adsorption of pure pyridine vapor for 20 min. The system was then evacuated at different temperatures and pyridine-adsorbed IR spectra were recorded.

Nitrogen adsorption–desorption measurements of the sulfided catalysts were performed on a Micromeritics ASAP 2002 adsorption instrument. The sulfided samples were degassed at 300 °C in a vacuum of 1.33×10^{-3} Pa for 15 h, and then switched to the analysis station for adsorption–desorption at liquid nitrogen tempera-

ture. The specific surface areas and pore volumes of the catalysts were calculated from N_2 adsorption–desorption isotherms using the Brunauer–Emmett–Teller (BET) and Barrett–Joyner–Halenda (BJH) methods.

IR spectra of adsorbed NO over the sulfided catalysts were measured using a FT-IR spectrometer (Nicolet Co., Magna 560). The pretreatment procedure for the oxidic catalyst samples was the same as that used in the above Py-FTIR measurement. After the background spectra were measured at a resolution of 4 cm^{-1}, the samples were exposed to a 10% NO/He stream for 0.5 h, followed by flushing with pure He for 1 h. Finally, the IR spectra of adsorbed NO were obtained by subtracting the background spectra.

IR spectra of adsorbed CO over the sulfided catalysts were measured using the same FT-IR spectrometer described above. The pretreatment procedure for the oxidic catalyst samples was the same as that used in the above Py-FTIR measurement. Then, the sulfided catalysts were rapidly evacuated at 300 °C and subsequently cooled to −173 °C for CO adsorption. Finally, the sulfided catalysts were exposed to CO with an equilibrium pressure of 133.3 Pa and the bands of the adsorbed CO species were obtained by subtracting the spectra recorded after and before CO introduction.

High-resolution transmission electron microscopy (HRTEM) images of the sulfided catalysts were obtained on a Philips Tecnai G2 F20 transmission electron microscope equipped with a Link-ISIS-300 energy-dispersive X-ray spectrometer (EDX) operated at an accelerating voltage of 200 kV. The solids to be measured were ultrasonically dispersed in cyclohexane and the testing samples were prepared by dropping the dispersed suspensions onto carbon-coated copper grids.

X-ray photoelectron spectroscopy (XPS) measurements of the sulfided catalysts were performed on a VG ESCA Lab 250 spectrometer using Al*K*α radiation. The oxidic catalysts were first sulfided in a 15% H_2S/H_2 stream at 360 °C for 3 h, cooled to room temperature in a He flow, ground, and then kept in cyclohexane to prevent oxidation. Before measurement, the sample to be tested was pressed onto a stainless steel sample holder and then the holder was immediately mounted on the XPS machine. The Al2*p* peak at 74.6 eV was used as an internal standard to compensate for sample charging. To quantify the content of W^{4+}, W^{5+}, and W^{6+} species, the obtained XPS spectra were fitted using XPSPEAK Version 4.1 software [29]. A Shirley background was applied, and the W4*f* spectra were deconvoluted by fitting the experimental spectra to a mixed Gaussian–Lorentzian function in which the Lorentzian function takes a fraction of 70–80% [13].

2.3. Catalyst assessment

The catalytic activity for 4,6-DMDBT HDS was assessed in a continuously flowing tubular fixed-bed microreactor of internal diameter 10.0 mm and length 500 mm, using 1.0 wt.% 4,6-DMDBT in *n*-decane as a model compound. A sample of 0.60 g of the catalyst to be assessed was diluted with quartz particles 0.25 mm in diameter to a constant volume of 2.0 ml before being loaded into the reactor. Before the reaction, the catalyst was presulfided for 3 h at 360 °C in a 15% H_2S/H_2 flow. The HDS reaction was carried out under the conditions of temperature 340 °C, a liquid hourly space velocity (LHSV) of 45 h^{-1}, a total pressure of 4.0 MPa, and a H_2/hydrocarbon volumetric ratio of 600. After a stabilization period of 4 h, the reaction products were collected and analyzed using an HP 6890 gas chromatograph (GC) installed with a flame ionization detector and a 0.25 mm × 100 m dimethylpolysiloxane capillary column. Some GC results were further verified by an HP 6890 GC installed with a pulse-flame photometric detector (O. I. Co., PFPD 5380) and by an HP 5790 GC installed with an MS 80 mass spectrometer.

By assuming a pseudo-first-order reaction for the HDS of 4,6-DMDBT, the catalyst activity can be expressed by the equation [30]

$$k_{HDS} = \frac{F}{m} \ln\left(\frac{1}{1-x}\right) \quad (1)$$

where x is the total conversion of 4,6-DMDBT, F is the molar feed rate of 4,6-DMDBT in mol s^{-1}, m is the catalyst mass in g, and k_{HDS} is the rate constant of HDS in mol g^{-1} s^{-1}. TOF (turnover frequency, s^{-1}) is defined as the number of reacted 4,6-DMDBT molecules per second and per W atom at the edge surface. This defined TOF represents the HDS efficiency of the W phase promoted by Ni (Ni–W–S) in view of the negligible HDS ability of the single promoter phase with a minor amount [31].

The HDS performance of the NiW/USY–Al_2O_3 catalysts was also evaluated using a coking diesel from a Chinese refinery with a boiling point in the range 200–395 °C, density 0.867 g cm^{-3}, and sulfur content 5350 μg g^{-1}. The HDS reaction for the coking diesel was conducted in a fixed-bed reactor loaded with 20 ml catalyst diluted with the same volume of quartz particles of diameter 0.25 mm. The catalysts were presulfided in a mixture of 3 wt.% CS_2 in cyclohexane. First, the sulfiding feed was introduced to wet the catalyst bed at 150 °C and 6.0 MPa for 1 h, and subsequently the bed temperature was increased to 230 °C and maintained there for 2 h; then the bed temperature was increased to 290 °C and maintained there for 2 h; finally, the bed temperature was increased to 360 °C and maintained there for 3 h. After sulfidation, the feeding flow was switched to the coking diesel, and the HDS assessment was carried out under the following conditions: LHSV 1.5 h^{-1}, temperature 360 °C, total pressure 6.0 MPa, and H_2/oil volume ratio 500. After steady state was achieved, the liquid product was collected for analysis.

3. Results and discussion

3.1. Py-FTIR and N_2 adsorption–desorption characterizations

The FT-IR spectra of pyridine adsorbed onto the catalysts CHD-HMY and IWI in the wavenumber range 1400–1600 cm^{-1} are shown in Fig. 1. The bands at 1545 and 1455 cm^{-1} correspond to pyridine molecules chemisorbed onto Brønsted (B) and Lewis (L) acid sites [32], respectively, and that at 1490 cm^{-1} is ascribed to the adsorbate on both B and L acid sites. Total L acidity and total B acidity, and medium and strong L acidity and medium and strong B acidity, can be calculated from the spectra of pyridine adsorption at 200 and 350 °C, respectively. The results for the acid-type distributions of the different catalysts from quantitative analysis by a method described elsewhere [33] are presented in Table 1. The hydrothermal treatment of the HY zeolite leads to the formation of nonframework Al species that conceal the B acid sites of the zeolite and thus restrain the access of pyridine molecules to them [34], but citric acid can remove the nonframework Al species formed during hydrothermal treatment by the chelation effect [35]. Therefore, catalyst CHD-HMY has more uncovered B acid sites than catalyst IWI due to the involvement of citric acid in the hydrothermal treatment. Similarly, fewer weak L acid sites over catalyst IWI than over catalyst CHD-HMY can be attributed mainly to the blockage of nonframework Al fragments in the pore channels of the support in the absence of citric acid. Compared with catalyst CHD-HMY, catalyst HD-HMY has fewer B acid sites, indicating the significant effect of citric acid on the exposure of B acid sites.

The pore structure parameters of the three catalysts listed in Table 2 show that relative to those of catalyst IWI, the surface area, pore volume, and average pore diameter of catalyst CHD-HMY are increased by about 20%, 32%, and 10%, respectively. The lower textural parameters of catalyst IWI compared to catalyst CHD-HMY can be attributed mainly to the blockage of more nonframework Al species in the pore channels of the hydrothermally treated support, because the surface area (264 m^2/g) and pore volume

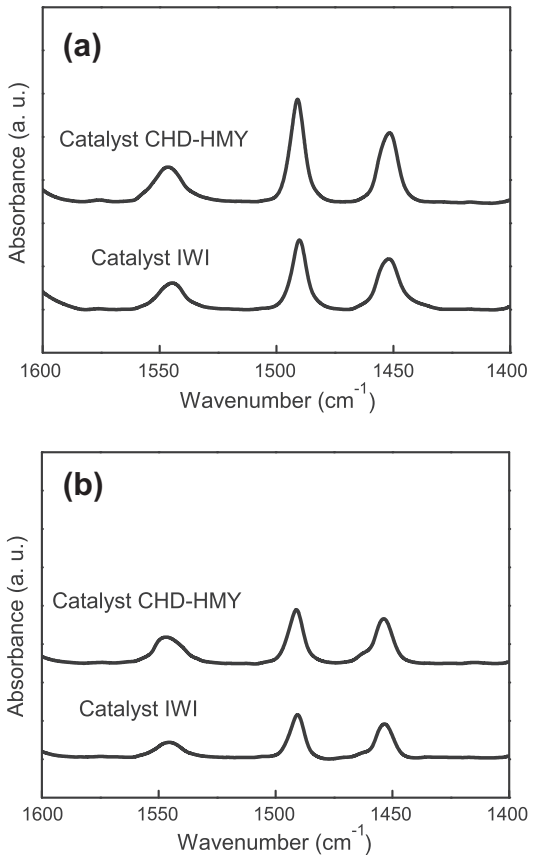

Fig. 1. FT-IR spectra of pyridine adsorbed on catalysts CHD-HMY and IWI at (a) 200 and (b) 350 °C, respectively.

Table 1
Acid type distributions of the three catalysts.

Catalyst	Acidity (μmol/g_{cat})					
	Weak acid sites		Medium and strong acid sites		Total amount	Total B/L
	L	B	L	B		
CHD-HMY	288.4	45.9	59.7	82.5	476.5	0.37
IWI	215.3	18.4	53.8	31.2	318.7	0.18
HD-HMY	232.8	20.6	55.2	39.1	347.7	0.21

(0.40 cm^3/g) of the support of catalyst IWI are lower than those (310 m^2/g, 0.52 cm^3/g) of the support of catalyst CHD-HMY with fewer nonframework Al species.

The more B acid sites and larger surface area for catalyst CHD-HMY than for catalyst HD-HMY demonstrate the important role citric acid plays in removing nonframework Al fragments generated in the hydrothermal treatment of the support, as well as the negligible effect of the matrix Al_2O_3 on protecting the framework Al species in the HY zeolite during the hydrothermal treatment.

3.2. TPR and XPS characterizations

The TPR profiles of the oxidic CHD-HMY and IWI catalysts are displayed in Fig. 2. The low-temperature peaks at 616 and 647 °C correspond to the reduction of octahedrally coordinated polymeric tungsten species [36], and the high-temperature peaks at 878 and 915 °C are attributed to the reduction of tetrahedrally coordinated monomeric tungsten species, which are mostly stabilized on the alumina-containing support [37]. Because the peak temperatures in the TPR profiles reflect the metal–support interaction over supported catalysts [38], the lower peak temperatures for catalyst CHD-HMY than for catalyst IWI in Fig. 2 indicate weaker metal–support interaction on the former catalyst. The weaker metal–support interaction over catalyst CHD-HMY originates from the preferential interaction between citric acid and the alumina-containing support [39], which can greatly improve the sulfidation of oxidic tungsten species, as further confirmed by the following XPS characterization results of the corresponding sulfided catalysts.

Table 2
Typical properties of the three catalysts.

Item	Catalyst CHD-HMY	Catalyst IWI	Percentage difference between catalysts CHD-HMY and IWI (%)	Catalyst HD-HMY
Pore parameter				
S_g[a] (m^2/g)	230	191	20	199
V_p[b] (cm^3/g)	0.41	0.31	32	0.33
D_p[c] (nm)	7.13	6.49	10	6.63
Surface W/Ni ratio[d]	2.69	1.86	45	1.97
$W_{sulfidation}$[d] (%)	78	64	18	67
$\overline{L}_{WS_2}$[e] (nm)	4.3	7.8	−45	6.5
$\overline{N}_{WS_2}$[e]	2.6	3.9	−36	3.3
WS_2 dispersion[e]	0.29	0.13	123	0.16

[a] BET surface area.
[b] Pore volume.
[c] Average pore diameter ($4V_p/S_g$).
[d] Obtained by XPS.
[e] Obtained by HRTEM.

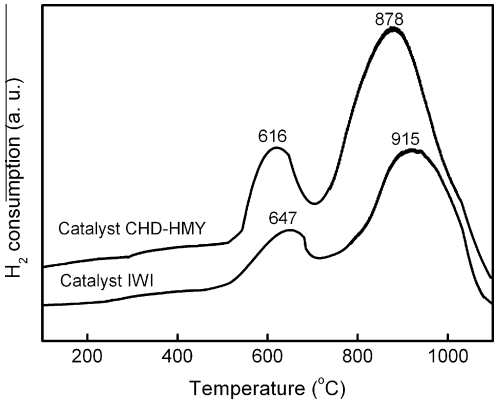

Fig. 2. TPR profiles of the oxidic CHD-HMY and IWI catalysts.

In view of the important influence of W sulfidation degree on the HDS activity of W-based catalysts, the W4*f* XPS spectra and deconvolutions of the sulfided CHD-HMY and IWI catalysts are shown in Fig. 3a. The binding energies of the W4$f_{7/2}$ and W4$f_{5/2}$ levels for W^{4+} (tungsten sulfides, WS_2) are about 32.2 and 34.3 eV, respectively, those for W^{5+} (tungsten oxysulfides, WOS) are about 32.9 and 34.8 eV, and those for W^{6+} (tungsten oxides, WO_3) are about 36.1 and 37.8 eV [40]. The sulfidation degree of oxidic W species, $W_{sulfidation}$, is defined as the ratio of $W^{4+}(WS_2)$ to the sum of $W^{4+}(WS_2)$, $W^{5+}(WOS)$, and $W^{6+}(WO_3)$; i.e., $W_{sulfidation} = W^{4+}/(W^{4+} + W^{5+} + W^{6+})$ [41]. The fitting results in Table 2 show that $W_{sulfidation}$ is 78% for catalyst CHD-HMY, 67% for catalyst HD-HMY, and 64% for catalyst IWI, respectively. Because $W_{sulfidation}$ depends inversely on the metal–support interaction [42], the highest $W_{sulfidation}$ of catalyst CHD-HMY among the three catalysts can be contributed to the weakest tungstate–support interaction.

In Fig. 3b, the decomposed Ni2*p* peaks at 856.6, 854.8 and 854.4, and 853.5 eV can be attributed to Ni oxides, the Ni–W–S

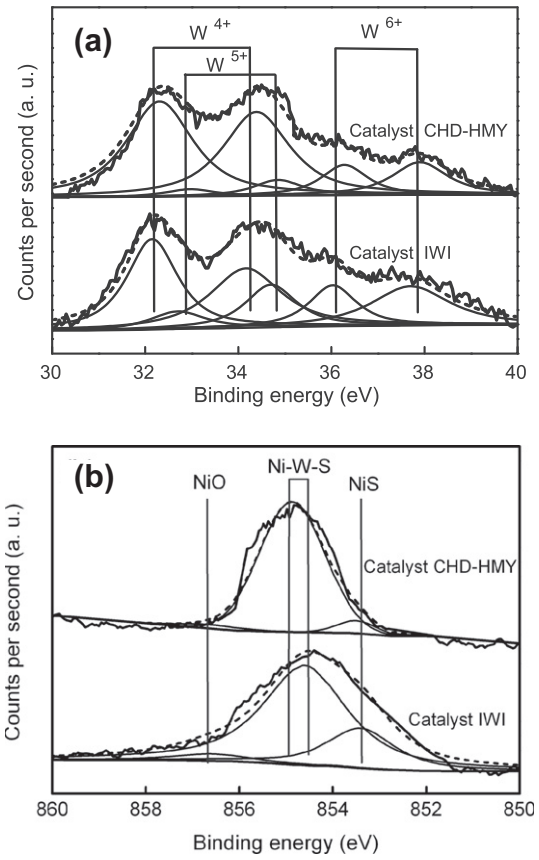

Fig. 3. W4*f* (a) and Ni2*p* (b) XPS spectra of the sulfided CHD-HMY and IWI catalysts.

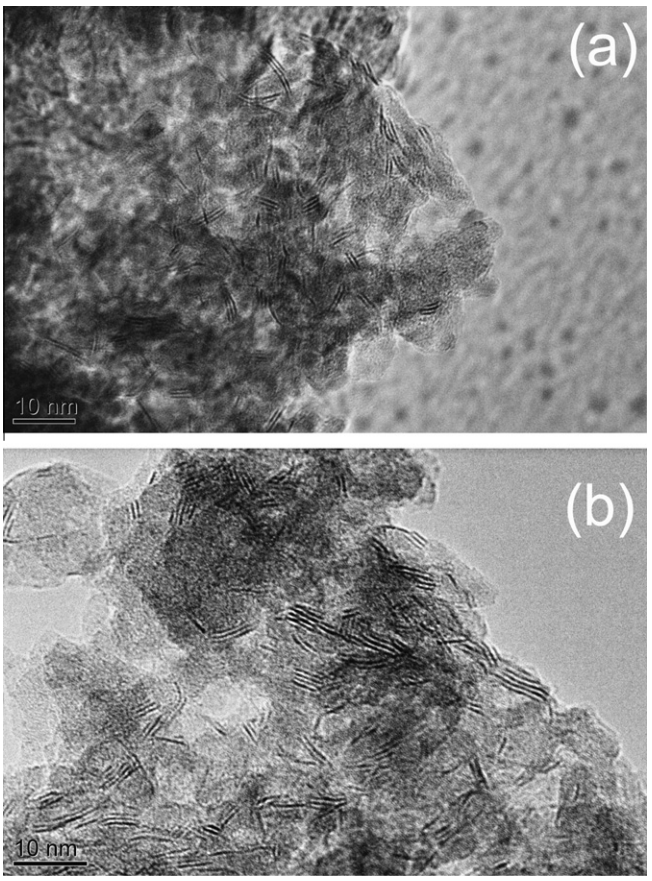

Fig. 4. HRTEM images of the sulfided catalysts (a) CHD-HMY and (b) IWI.

phases in which Ni atoms neighbor W atoms with electron transfer from Ni to adjacent WS_2, and Ni sulfides, respectively [28,43]. The very low peak intensity at 856.6 eV indicates a very low content of Ni oxides over the sulfided CHD-HMY and IWI catalysts, and the high peak intensities at 854.8 and 854.4 eV reveal that Ni–W–S phases exist in the majority over the two sulfided catalysts. In addition, the higher Ni2*p* peak at 853.5 eV over catalyst IWI than over catalyst CHD-HMY demonstrates the coexistence of more Ni sulfides with the Ni–W–S phases over the former catalyst, as reported in the literature [44].

The surface W/Ni atomic ratios of the different sulfided catalysts were also measured by XPS and the results are given in Table 2. Despite the same metal contents over the three catalysts as determined by XRF, catalyst CHD-HMY has the highest surface W/Ni atomic ratio, indicating the smallest size of the supported W species over catalyst CHD-HMY [45].

3.3. HRTEM characterization

Representative HRTEM micrographs of the sulfided CHD-HMY and IWI catalysts are shown in Fig. 4. They mainly display the edge or prism planes of WS_2 slabs on the two catalysts orienting along or roughly parallel to the electron beam direction [46]. The black thread-like fringes correspond to WS_2 slabs (confirmed by the EDX analysis). The particles of the promoter Ni species on the sulfided catalysts are too small to be visualized in the HRTEM images due to the very low loading of Ni species, in accordance with literature results [44].

To make a quantitative comparison, the lengths and layer numbers of WS_2 slabs on the sulfided catalysts were obtained through statistical analyses based on about 20 micrographs, including 500–600 slabs taken from different parts of each catalyst. The average slab length ($\bar{L}$) and stacking layer number ($\bar{N}$) were calculated according to the first moment of the distribution [22,43], expressed by

$$\bar{L}(\bar{N}) = \frac{\sum_{i=1}^{n} x_i M_i}{\sum_{i=1}^{n} x_i}, \quad (2)$$

where M_i is the slab length or stacking layer number of a stacked WS_2 unit, and x_i the number of slabs or stacks in a given range of lengths or stacking layer numbers.

Table 3
Length and stacking layer number distributions of the WS_2 slabs over the sulfided CHD-HMY and IWI catalysts.

	Frequency (%)	
	CHD-HMY	IWI
Length (nm)		
<2	15.6	1.6
2–4	29.5	5.2
4–6	40.3	8.0
6–8	8.9	38.3
8–10	5.5	32.1
10–12	0.2	14.8
Stacking layer number		
1	10.2	1.7
2	32.5	8.5
3	47.6	14.4
4	5.7	52.7
5	3.3	17.8
6	0.7	4.9

The statistical results of the length and stacking layer number distributions of WS_2 slabs over the sulfided CHD-HMY and IWI catalysts are displayed in Table 3. CHD-HMY significantly decreases the fraction of WS_2 slabs larger than 6 nm and greatly increases the fraction of WS_2 slabs smaller than 4 nm, resulting in a decrease of the average slab length from 7.8 nm for catalyst IWI to 4.3 nm for catalyst CHD-HMY (Table 2). In addition, catalyst CHD-HMY has more WS_2 slabs stacked with 1–3 layers and fewer stacked with 4–6 layers than catalyst IWI, leading to an increase of the average stacking layer number from 2.6 for the former to 3.9 for the latter (Table 2). The average length and stacking layer number of WS_2 slabs over catalyst IWI are higher than those over the impregnated NiW/Al_2O_3 catalysts reported in literatures [43,44], indicating that the incorporation of USY into Al_2O_3 deteriorates the dispersion of supported WS_2 slabs.

The WS_2 dispersion, f_W, was calculated by dividing the total number of W atoms at the edge surface by the total number of W atoms. By assuming that WS_2 slabs are present as perfect hexagons, the following equation was derived [47],

$$f_W = \frac{\sum_{i=1,\ldots,t}(6n_i - 6)}{\sum_{i=1,\ldots,t}(3n_i^2 - 3n_i + 1)}, \quad (3)$$

where n_i is the number of W atoms along one edge of a WS_2 slab determined from its length ($L = 3.2(2n_i - 1)$ Å), and t is the total number of slabs shown in the TEM micrographs.

The calculation results for WS_2 dispersion in Table 2 show that the WS_2 dispersion over the different catalysts decreases in the order catalyst CHD-HMY > catalyst HD-HMY > catalyst IWI. Among the three catalysts, the highest WS_2 dispersion over catalyst CHD-HMY can efficiently promote the occupation of Ni atoms on the edge sites of WS_2 slabs and thus greatly favor the formation of Ni–W–S active phases [48].

The statistical results of the HRTEM micrographs for catalyst IWI-IC reveal that the WS_2 slabs have an average length of 8.7 nm, an average stacking layer number of 4.1, and a dispersion of 0.10, indicating that citric acid can hardly enhance the dispersion of W species during the conventional impregnation process. In W-containing catalyst preparation by conventional impregnation, ammonium metatungstate [$(NH_4)_6H_2W_{12}O_{40}$] with polymeric tungstates is generally used as the W precursor. It is known that polymeric W species (W_{12}) are absolutely predominant in solution in the case of pH < 3.5 [49], so the W precursors in the citric acid-containing impregnation solution for preparing catalyst IWI-IC exist in the form of the polymeric W species (W_{12}) when the solution pH value is at 2.0 (measured on a Mettler-Toledo Delta 320 pH meter). In this case, the advantages of citric acid in improving the dispersion of supported W species are greatly diminished due to the preferential formation of polymeric W species (W_{12}). Differently, in the CHD-HMY method the H_2WO_4 precipitates in the form of monomeric W species, i.e., hydrated WO_3 particles, are generated through the stoichiometric reaction between Na_2WO_4 and HCl, and they are well dispersed because of the multiple effects of citric acid: the hydrogen-bonding interaction between the carboxyl groups of citric acid and the $(WO_n)^-$ anions adsorbed on the surfaces of the hydrated WO_3 particles [50], the decreased capillary forces between WO_3 particles during the drying step [51], and the preserved dispersion of oxidic W species during the calcination under N_2 due to the remnant carbonaceous species and gases released from the decomposition of citric acid [52,53].

The statistical results of the HRTEM micrographs for catalyst IWI-HC display that the WS_2 slabs have an average length of 7.6 nm, an average stacking layer number of 4.0, and a dispersion of 0.14, demonstrating that citric acid can hardly improve the dispersion of W species when incorporated into the hydrothermal solution for producing the USY zeolite used in catalyst IWI. This is because the predominance of the polymeric W species (W_{12}) in the impregnation solution of $(NH_4)_6H_2W_{12}O_{40}$ with a pH value of 3.1 leads to inferior W dispersion, as discussed above.

During the IWI process, the existence of polymeric W species in the impregnating solution and the undesirable agglomeration of metal species in the drying and calcination steps deteriorate the dispersion of active metal species on the support, as demonstrated by the above XPS and HRTEM characterizations.

3.4. NO-IR and CO-IR characterizations

IR spectra of adsorbed NO on the sulfided catalysts are shown in Fig. 5. The bands at about 1844 and 1782 cm^{-1} are assigned to NO adsorbed onto Ni and W species [54], respectively. Obviously, catalyst CHD-HMY has a higher peak intensity of Ni species and a lower peak intensity of W species than catalyst IWI. This can be ascribed to the following reason: Ni species preferentially interact with W species rather than with alumina in $NiW/USY–Al_2O_3$ and thus the supported WS_2 slabs can be considered as the secondary support for Ni species [55]. As confirmed by the above XPS and HRTEM characterization results, WS_2 slabs have better dispersion over catalyst CHD-HMY than over catalyst IWI and thus provide more sites for accommodating the Ni species, so the number of WS_2 edge sites over catalyst CHD-HMY decreases remarkably due to the occupation of Ni species, and many dispersed and exposed Ni sites are formed in the Ni–W–S phases. It has been demonstrated that the HDS activity of supported metal catalysts is closely related to the Ni or Co sites present as Co(Ni)–Mo(W)–S phases [56], so catalyst CHD-HMY with more Ni sites in supported Ni–W–S phases is expected to have higher HDS activity than catalyst IWI.

IR spectra of adsorbed CO on the sulfided catalysts are shown in Fig. 6. The bands at 2133 and 2120 cm^{-1} are assigned to CO adsorbed onto the Ni promoter involved in the Ni–W–S phases and the bands at 2099 and 2088 cm^{-1} are associated with CO adsorbed onto the WS_2 phases perturbed by Ni [42]. Similarly to the above NO-IR results, catalyst CHD-HMY has a higher peak intensity of Ni species and a lower peak intensity of W species than catalyst IWI. It should be pointed out that the υ(CO) wavenumber increases from 2120 and 2088 cm^{-1} for catalyst IWI to 2133 and 2099 cm^{-1} for catalyst CHD-HMY, respectively. This shift to higher energies normally corresponds to the increased electron deficiency of metal species [57], and can be attributed to the enhanced induction effect of more exposed B acid sites over catalyst CHD-HMY [17]. In addition, the bands at 2190, 2176, and 2159 cm^{-1} in Fig. 6 are ascribed to the interactions of CO with L acid sites, B acid sites, and Al–OH groups of the support, respectively [17,43]. Catalyst CHD-HMY has higher peak intensities at 2190 and 2176 cm^{-1} than catalyst IWI, indicating more L and B acid sites over the former's support than

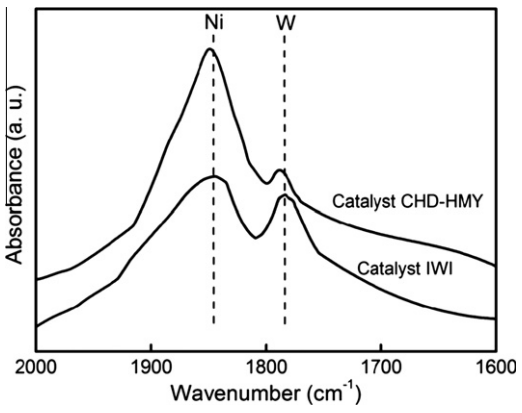

Fig. 5. IR spectra of adsorbed NO on the sulfided CHD-HMY and IWI catalysts.

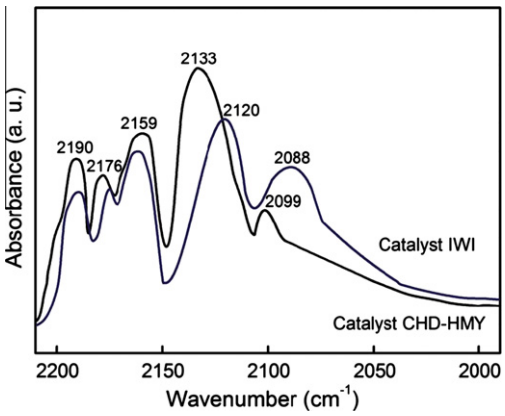

Fig. 6. IR spectra of adsorbed CO on the sulfided CHD-HMY and IWI catalysts.

over the latter's support. It is the blockage of nonframework Al fragments generated in the hydrothermal treatment that leads to fewer exposed L and B acid sites in the support of catalyst IWI, as pointed out in the above Py-FTIR characterization.

3.5. Catalytic activity

As shown in Fig. 7, the reaction network of 4,6-DMDBT HDS includes four routes [20,58]: (1) the dealkylation route, in which the methyl groups at the 4 and/or 6 positions are removed by cracking and then sulfur is eliminated by hydrogenolysis; (2) the direct desulfurization (DDS) route, in which the C–S bonds of the reactant molecule are broken by hydrogenolysis, yielding 3,3′-dimethylbiphenyl (3,3′-DMBP); (3) the isomerization route, in which the methyl groups at the 4 and/or 6 positions are transferred to the other positions and then sulfur is eliminated by hydrogenolysis; (4) the hydrogenation (HYD) route, in which the reactant molecules are first hydrogenated to tetrahydrodimethyldibenzothiophene (4,6-THDMDBT) and then to hexahydrodimethyldibenzothiophene (4,6-HHDMDBT) intermediates, and finally sulfur is eliminated from these intermediates, producing methylcyclohexyltoluene (3,3′-MCHT) and hydrogenated dimethylbicyclohexyl (3,3′-DMBCH). Due to the absence of the dealkylation and isomerization routes here, the HDS/HYD ratio can be calculated by dividing the total selectivity to 3,3′-MCHT, 3,3′-DMBCH, and 3,3′-DMBP by the total selectivity to 4,6-THDMDBT, 4,6-HHDMDBT, 3,3′-MCHT, and 3,3′-DMBCH.

The 4,6-DMDBT HDS results for the catalysts in Table 4 show that the reaction rate constant and the TOF over catalyst CHD-HMY are higher than those over catalyst IWI, revealing the higher activity of the former catalyst for transforming 4,6-DMDBT. The 3,3′-MCHT selectivity over catalyst CHD-HMY is much higher than that over catalyst IWI, indicating the superior HDS activity of the former catalyst by the HYD route, but the 3,3′-DMBP selectivities over the two catalysts have only a minor difference due to the steric hindrance effect of 4,6-DMDBT on the DDS route [59]. More-

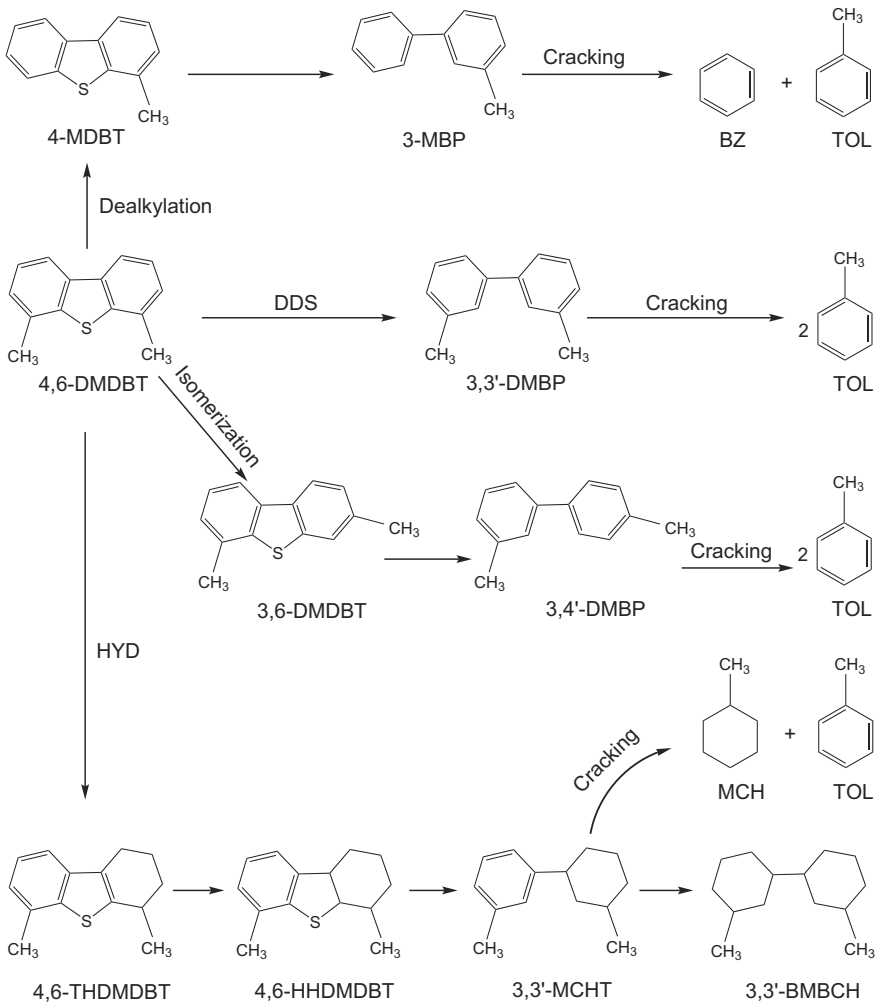

Fig. 7. Reaction network of 4,6-DMDBT HDS.

Table 4
4,6-DMDBT HDS results over the three sulfided catalysts.

Catalyst	k_{HDS} (10^{-7} mol g^{-1} s^{-1})	TOF × 10^4 (s^{-1})[a]	Product selectivity[b] (%)					
			4,6-THDMDBT + 4,6-HHDMDBT	3,3′-MCHT	3,3′-DMBCH	3,3′-DMBP	HDS/HYD[c]	(4,6-THDMDBT + 4,6-HHDMDBT)/3,3′-MCHT
CHD-HMY	4.97	10.32	12.5	69.2	8.7	9.6	0.97	0.18
IWI	0.52	3.43	30.9	54.1	4.2	10.8	0.77	0.57
HD-HMY	0.82	4.27	25.3	58.7	5.9	10.1	0.83	0.43

[a] The number of reacted 4,6-DMDBT molecules per second and per W atom at the edge surface.
[b] Determined at about 50% of total 4,6-DMDBT conversion by changing the liquid hourly space velocity.
[c] Obtained via dividing the total selectivity to 3,3′-MCHT, 3,3′-DMBCH and 3,3′-DMBP by the total selectivity to 4,6-THDMDBT, 4,6-HHDMDBT, 3,3′-MCHT, and 3,3′-DMBCH.

over, the HDS/HYD ratio over catalyst CHD-HMY is higher than that over catalyst IWI, implying better HDS selectivity of the former catalyst for the HYD route. It is also noted that the total selectivity to 4,6-THDMDBT and 4,6-HHDMDBT and the (4,6-THDMDBT + 4,6-HHDMDBT)/3,3′-MCHT ratio over catalyst CHD-HMY are lower than those over catalyst IWI, showing the superior hydrogenolysis desulfurization capability of the former catalyst.

Compared with catalyst CHD-HMY, catalyst HD-HMY has a lower reaction rate constant and TOF as well as an inferior desulfurization capability (Table 4), indicating the significance of citric acid in enhancing the HDS performance of catalyst CHD-HMY.

With the real coking diesel as feedstock, the activity stabilities of catalysts CHD-HMY and IWI were assessed and the results are presented in Fig. 8 and Table 5. During the operation of 400 h, the total sulfur content in the products obtained over the two catalysts remained stable, with the sulfur content in the product obtained over catalyst CHD-HMY much lower than that in the product over catalyst IWI, indicating the advantageous HDS performance of catalyst CHD-HMY.

The above assessment results of 4,6-DMDBT and real coking diesel HDS have confirmed that catalyst CHD-HMY has higher HDS activity than catalyst IWI. To further compare their activity, it is necessary to correlate the HDS activities of the two catalysts with their structures.

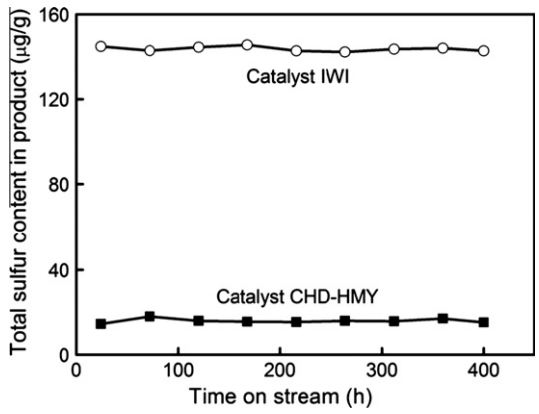

Fig. 8. Total sulfur content in the diesel products with time on stream over the sulfided CHD-HMY and IWI catalysts.

Table 5
Coking diesel HDS results over catalysts CHD-HMY and IWI.

Catalyst	Total sulfur content in feedstock (μg/g)	Average of total sulfur content in product (μg/g)	HDS ratio (%)
CHD-HMY	5350	15.7	99.7
IWI	5350	144.5	97.3

According to literature results [60,61] and those obtained in the present investigation, it is proposed that in the supported Ni–W–S phase the brim sites (i.e., the top and bottom layers of multistacks) are HYD-oriented and the edge sites are DDS-oriented. Compared with catalyst IWI, catalyst CHD-HMY with a WS_2 dispersion of 0.29 and an average WS_2 stacking number of 2.6 (Table 2) has more accessible Ni–W–S active sites, as confirmed in Figs. 5 and 6, so its prehydrogenation activity for the refractory 4,6-DMDBT with steric hindrance is remarkably enhanced due to the presence of more accessible brim sites (Fig. 9). The molecules 4,6-THDMDBT and 4,6-HHDMDBT as the hydrogenated intermediates of 4,6-DMDBT have no such steric hindrance as the initial 4,6-DMDBT, and thus their C–S bond cleavage by hydrogenolysis on the edge sites of Ni–W–S phases is much easier than that of 4,6-DMDBT (Fig. 9). As a result, catalyst CHD-HMY with more accessible edge sites shows the much higher 3,3′-MCHT selectivity than catalyst IWI.

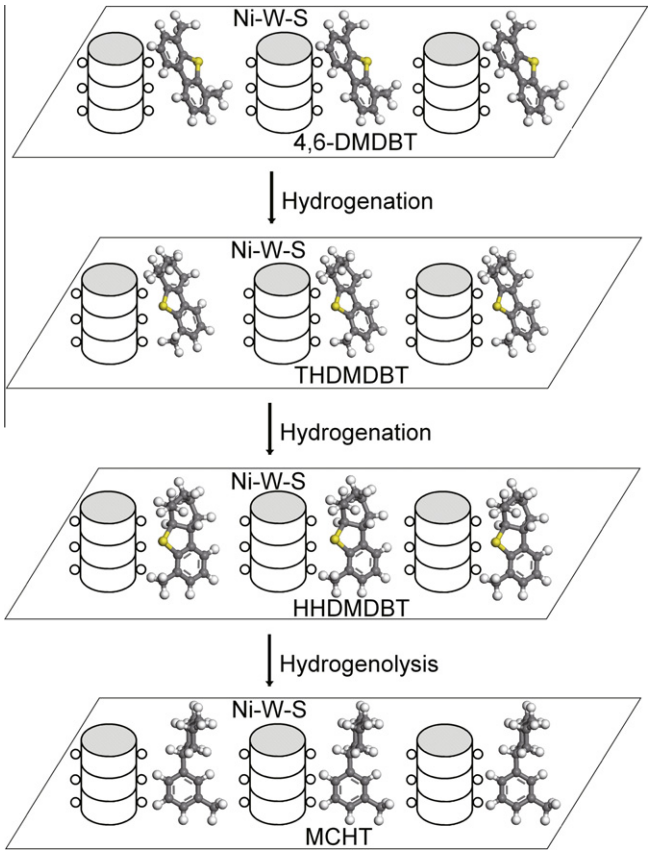

Fig. 9. Schematic representation for eliminating steric hindrance of 4,6-DMDBT via the HYD route over the sulfided CHD-HMY catalyst with the compromised dispersion and stacking of Ni–W–S phases.

The promoting impacts of zeolites on 4,6-DMDBT HDS are attributed to isomerization, dealkylation, or electronic effects [62]. In our case, no isomerization or cracking products of 4,6-DMDBT are detected, and thus the electronic effect induced by B acid sites in the zeolite should be pursued. It has been recognized that B acidity can enhance the electronic deficiency of active Ni–W–S phases, as proved by a blue shift in the position of the $\upsilon(CO–NiWS_x)$ band caused by the support B acidity [17,58], and the increased electronic deficiency improves the HDS ability of zeolite-containing catalysts [63]. Therefore, catalyst CHD-HMY, with a higher electronic deficiency of Ni–W–S phases, as confirmed by the above CO-IR results, has higher activity for 4,6-DMDBT HDS than catalyst IWI.

4. Conclusions

By coupling the citric acid-assisted hydrothermal dispersion of supported metals and the hydrothermal modification of HY zeolite, a novel method for preparing NiW/USY–Al_2O_3 ultradeep hydrodesulfurization (HDS) catalysts was proposed. Different from the conventional impregnation method that uses polymeric W species as W precursors, this method yielded monomeric W species as W precursors and achieved excellent dispersion of these monomeric W species via (1) the hydrogen-bonding interaction between the carboxyl groups of citric acid and the WO_3 particles, (2) the decreased capillary forces between WO_3 particles caused by the adsorption of citric acid during the drying step, and (3) the greatly restrained aggregation of WO_3 particles through the separating effect of the remnant carbonaceous species and released gases from the decomposition of citric acid during the calcination step. This method also weakened the metal–support interaction due to the preferential interaction between the carboxyl groups of citric acid and the surface hydroxyls on the support. The combined effects provided the resulting catalyst with better dispersed and less stacked Ni–W–S active phases. Moreover, during the citric acid-assisted hydrothermal process, the acidity and pore structure of the USY zeolite were simultaneously tuned, which reopens the pore channels blocked by nonframework alumina species due to the dealumination of the HY zeolite and thus exposes more Brønsted acid sites. The finely tuned morphology of the Ni–W–S active phases via the citric acid-assisted hydrothermal process and the increased electron deficiency of the Ni–W–S phases induced by more Brønsted acid sites from the incorporated USY zeolite significantly improved the hydrogenation route of 4,6-DMDBT HDS, endowing the corresponding catalyst with ultradeep HDS performance.

Acknowledgments

This work was supported by the National Basic Research Program of China (Grant 2010CB226905), the Program for New Century Excellent Talents in University (Grant NCET-09-0763), the National Natural Science Foundation of China (Grants 21076228 and 20825621), and the Nova Program of Beijing (Grant 2007B073).

References

[1] M. Breysse, G. Djega-Mariadassou, S. Pessayre, C. Geantet, M. Vrinat, G. Pérot, et al., Catal. Today 84 (2003) 129.
[2] F. Bataille, J.L. Lemberton, P. Michaud, G. Pérot, M. Vrinat, M. Lemaire, et al., J. Catal. 191 (2000) 409.
[3] C. Song, X. Ma, Appl. Catal. B Environ. 41 (2003) 207.
[4] K.V.R. Chary, H. Ramakrishna, G.M. Dhar, J. Mol. Catal. 68 (1991) L25.
[5] A.K. Datye, S. Srinivasan, L.F. Allard, C.H.F. Peden, J.R. Brenner, L.T. Thompson, J. Catal. 158 (1996) 205.
[6] S.K. Maity, M.S. Rana, B.N. Srinivas, S.K. Bej, G. Muralidhar, T.S.R. Prasada Rao, J. Mol. Catal. A Chem. 153 (2000) 121.
[7] Y. Okamoto, K. Ochiai, M. Kawano, K. Kobayashi, T. Kubota, Appl. Catal. A Gen. 226 (2002) 115.
[8] M.S. Rana, J. Ancheyta, S.K. Maity, P. Rayo, Catal. Today 109 (2005) 61.
[9] C. Leyva, M.S. Rana, J. Ancheyta, Catal. Today 130 (2008) 345.
[10] G. Li, W. Li, M. Zhang, K. Tao, Appl. Catal. A Gen. 273 (2004) 233.
[11] G.M. Dhar, B.N. Srinivas, M.S. Rana, M. Kumar, S.K. Maity, Catal. Today 86 (2003) 45.
[12] H. Kraus, R. Prins, J. Catal. 170 (1997) 20.
[13] M. Sun, T. Burgi, R. Cattaneo, D. van Langeveld, R. Prins, J. Catal. 201 (2001) 258.
[14] G. Kishan, L. Coulier, V.H.J. de Beer, J.A.R. van Veen, J.W. Niemantsverdriet, J. Catal. 196 (2000) 180.
[15] M.A. Lélias, P.J. Kooyman, L. Mariey, L. Oliviero, A. Travert, J. van Gestel, et al., J. Catal. 267 (2009) 14.
[16] M. Sun, D. Nicosia, R. Prins, Catal. Today 86 (2003) 173.
[17] C.E. Hédoire, C. Louis, A. Davidson, M. Breysse, F. Maugé, M. Vrinat, J. Catal. 220 (2003) 433.
[18] M. Breysse, M. Cattenot, V. Kougionas, J.C. Lavalley, F. Maugé, J.L. Portefaix, et al., J. Catal. 168 (1997) 143.
[19] P. Michaud, J.L. Lemberton, G. Pérot, Appl. Catal. A Gen. 169 (1998) 343.
[20] M.V. Landau, D. Berger, M. Herskowitz, J. Catal. 159 (1996) 236.
[21] S.K. Bej, S.K. Maity, U.T. Turaga, Energy Fuel 18 (2004) 1227.
[22] L. Ding, Y. Zheng, Z. Zhang, Z. Ring, J. Chen, J. Catal. 241 (2006) 435.
[23] F. Bataille, J.L. Lemberton, G. Pérot, P. Leyrit, T. Cseri, N. Marchal, et al., Appl. Catal. A Gen. 220 (2001) 191.
[24] L. Ding, Y. Zheng, Z. Zhang, Z. Ring, J. Chen, Catal. Today 125 (2007) 229.
[25] N. Kunisada, K.H. Choi, Y. Korai, I. Mochida, K. Nakano, Appl. Catal. A Gen. 276 (2004) 51.
[26] J. Léglise, J.M. Manoli, C. Potvin, G. Djega Mariadassou, D. Cornet, J. Catal. 152 (1995) 275.
[27] J.A. Anderson, B. Pawelec, J.L.G. Fierro, P.L. Arias, F. Duque, J.F. Cambra, Appl. Catal. 99 (1993) 55.
[28] L. Zhang, P. Afanasiev, D. Li, X. Long, M. Vrinat, Catal. Today 130 (2008) 24.
[29] E.J.M. Hensen, V.H.J. de Beer, J.A.R. van Veen, R.A. van Santen, Catal. Lett. 84 (2002) 59.
[30] M.P. De la Rosa, S. Texier, G. Berhault, A. Camacho, M.J. Yácaman, A. Mehta, et al., J. Catal. 225 (2004) 288.
[31] M.V. Landau, L. Vradman, M. Herskowitz, Y. Koltypin, A. Gedanken, J. Catal. 201 (2001) 22.
[32] J.A.Z. Pieterse, S. Veefkind-Reyes, K. Seshan, L. Domokos, J.A. Lercher, J. Catal. 187 (1999) 518.
[33] Y. Fan, D. Lei, G. Shi, X. Bao, Catal. Today 114 (2006) 388.
[34] N. Salman, C.H. Rüscher, J.C. Buhl, W. Lutz, H. Toufar, M. Stöcker, Micropor. Mesopor. Mater. 90 (2006) 339.
[35] X. Liu, Z. Yan, Catal. Today 68 (2001) 145.
[36] D.C. Vermaire, P.C. van Berge, J. Catal. 116 (1989) 309.
[37] B. Scheffer, P. Molhoek, J.A. Moulijn, Appl. Catal. 46 (1989) 11.
[38] Y. Fan, X. Bao, H. Wang, C. Chen, G. Shi, J. Catal. 245 (2007) 477.
[39] K.D. Dobson, A.J. McQuillan, Spectrochim. Acta Part A 55 (1999) 1395.
[40] L. Qiu, G. Xu, Appl. Surf. Sci. 256 (2010) 3413.
[41] B. Pawelec, R. Mariscal, J.L.G. Fierro, A. Greenwood, P.T. Vasudevan, Appl. Catal. A Gen. 206 (2001) 295.
[42] H. Wang, Y. Fan, G. Shi, H. Liu, X. Bao, J. Catal. 260 (2008) 119.
[43] D. Zuo, M. Vrinat, H. Nie, F. Maugé, Y. Shi, M. Lacroix, et al., Catal. Today 93–95 (2004) 751.
[44] D. Zuo, D. Li, H. Nie, Y. Shi, M. Lacroix, M. Vrinat, J. Mol. Catal. A Chem. 211 (2004) 179.
[45] J.J. Lee, H. Kim, J.H. Koh, A. Jo, S.H. Moon, Appl. Catal. B Environ. 58 (2005) 89.
[46] A. Sampieri, S. Pronier, J. Blanchard, M. Breysse, S. Brunet, K. Fajerwerg, et al., Catal. Today 107–108 (2005) 537.
[47] E.J.M. Hensen, P.J. Kooyman, Y. van der Meer, A.M. van der Kraan, V.H.J. de Beer, J.A.R. van Veen, et al., J. Catal. 199 (2001) 224.
[48] L. Vradman, M.V. Landau, Catal. Lett. 77 (2001) 47.
[49] L. Karakonstantis, K. Bourikas, A. Lycourghiotis, J. Catal. 162 (1996) 295.
[50] M. Sun, N. Xu, Y.W. Cao, J.N. Yao, E.G. Wang, J. Mater. Sci. Lett. 19 (2000) 1407.
[51] A.P. Hyvärinen, H. Lihavainen, A. Gaman, L. Vairila, H. Ojala, M. Kulmala, et al., J. Chem. Eng. Data 51 (2005) 255.
[52] Z. Lu, S.M. Kanan, C.P. Tripp, J. Mater. Chem. 12 (2002) 983.
[53] P. Afanasiev, G. Xia, G. Berhault, B. Jouguet, M. Lacroix, Chem. Mater. 11 (1999) 3216.
[54] A. Benítez, J. Ramírez, J.L.G. Fierro, A. López Agudo, Appl. Catal. A Gen. 144 (1996) 343.
[55] S.P.A. Louwers, R. Prins, J. Catal. 139 (1993) 525.
[56] N.Y. Topsøe, H. Topsøe, J. Catal. 84 (1983) 386.
[57] A. Travert, C. Dujardin, F. Maugé, E. Veilly, S. Cristol, J.F. Paul, et al., J. Phys. Chem. B 110 (2005) 1261.
[58] S. Zeng, J. Blanchard, M. Breysse, Y. Shi, X. Su, H. Nie, et al., Appl. Catal. A Gen. 298 (2006) 88.
[59] O.Y. Gutiérrez, D. Valencia, G.A. Fuentes, T. Klimova, J. Catal. 249 (2007) 140.
[60] M. Daage, R.R. Chianelli, J. Catal. 149 (1994) 414.
[61] F. Besenbacher, M. Brorson, B.S. Clausen, S. Helveg, B. Hinnemann, J. Kibsgaard, et al., Catal. Today 130 (2008) 86.
[62] G. Pérot, Catal. Today 86 (2003) 111.
[63] M. Breysse, C.E. Hédoire, C. Louis, G. Pérot, Stud. Surf. Sci. Catal. 145 (2003) 115.